PHASE SEGREGATION IN SWIRLING FLOW AXIAL HYDROCYCLONE

André D. Rocha, damiani@dep.fem.unicamp.br
Antonio C. Bannwart, bannwart@dep.fem.unicamp.br
State University of Campinas – UNICAMP-FEM-DEP
Dept. of Petroleum Engineering
Cidade Universitária – B. Geraldo
13083-970 – Campinas-SP-Brazil

Marcelo M. Ganzarolli, ganza@fem.unicamp.br
State University of Campinas – UNICAMP-FEM-DE
Dept. of Energy
Cidade Universitária – B. Geraldo
13083-970 – Campinas-SP-Brazil

Abstract. Oil-water separators are often required in process industries and are essential in offshore petroleum production. A compact design is provided by the axial hydrocyclone, which takes advantage of the pipe geometry of the incoming oil-water mixture. In light oil applications, the objective is simply to remove water dispersed into the oil, whereas for heavy oil the hydrocyclone may further be thought as a core-flow generator. In this work, the phase segregation capability of the swirling oil-water flow presume at the hydrocyclone inlet is investigated. A flow pattern of small water droplet in the swirling flow was investigated. The equations of the motion of the droplet are solved numerically, by assuming that the droplet behaves as a solid sphere of small size and does not modify the oil flow. A simplified analytical model was also developed to predict the droplet trajectory. Different droplet sizes, and inlet swirling angles were simulated for laminar oil Reynolds number. Numerical solutions for the particle trajectory and evolution of the swirling number along an essentially cylindrical hydrocyclone was obtained by means of a CFD code and compared to the analytical solutions. The agreement was found to be satisfactory and allows the use of the numerical code in more complex geometries.

Keywords: oil-water separators, petroleum engineering, oil-water flow

1. INTRODUCTION

Cyclones are used in various industries to separate two components of different densities with the help of centrifugal forces created by the swirling flow. It is common to find solid-liquid and solid-gas cyclones in industry, but in the case of two immiscible liquids the application of hydrocyclones is less common due to the small density difference between the phases. One exception to this is the oil industry in which hydrocyclones are used to remove oil from the produced water before the aqueous phase is disposed overboard or re-injected into the formation.

The design of cyclones in general is still largely based on geometrical relationships and correlations obtained from experimental studies in a specific geometry or different geometries (Young *et al*., 1994). In a conventional cyclone the mixture to be separated enters the separation chamber via one or sometimes several inlets. Although the axial cyclone is less common, a number of designs can be found in several industrial applications, e.g. liquid removal from gas streams (Swanborn, 1988), solid/dust removal from gas (Klujszo *et al*., 1999). The application of axial hydrocyclones to liquid-liquid separation is very rare (Dirkzwager, 1996; Delfos and Dirkzwager, 1998). The flow along the axial hydrocyclone is put into rotation by a swirl generator device. This is a cylindrical body centered in the pipe, on which vanes are mounted in order to provide a tangential velocity component to the incoming axial flow. The difficulty in designing efficient hydrocyclones lies in the broad range of industrial applications, where for each set of physical operational parameters there is supposedly a different optimal geometry.

Dirkzwager (1996) has also developed an expression to predict the trajectory of the particles of dispersed oil in water flows. The author found that oil particles larger than $30\mu m$ of diameter have a 100% migration probability to the centre, i.e. they reach the centre of the pipe whatever their initial position. The study suggests the possibility of applying the model for dispersed water in oil flows too. Delfos (2004) developed a numerical model for liquid-liquid turbulent flow (called HAAS) to predict the velocity field in axi-symmetric flows with high swirl and Reynolds numbers in cyclone geometries. The results were compared with both simulations using a commercial CFD code (FLUENT) and results from laboratory experiments. A series of tracks of $5\mu m$ droplets released at a range of radial locations was obtained too. According to the author, the trajectories calculated by the code were inconclusive.

No investigation on viscous effects in axial hydrocyclones was found, although viscosity surely plays an important effect for heavy oils containing small dispersed water droplets. In this paper we numerically investigate the laminar and turbulent swirling flow in the downstream portion of a swirl generator, i.e. the so-called separation section or settling zone shown in Fig. 1. The numerical study is aimed at determining the phase segregation parameters, the required length for segregation and the length at which swirl motion decays as a function of the flow and geometry variables

involved. The decay length is compared with an approximate expression for the length required to segregate water droplets, as a criterion to assess the viability of a particular design.

2. FLOW FIELD OF THE CONTINUOUS PHASE

The swirling flow is governed by the fundamental principles of classical fluid mechanics, expressing the balances of mass and momentum. The flow geometry is illustrated in Fig. 1. For the continuous phase (e.g. oil), the corresponding equations for steady state, incompressible, isothermal and axi-symmetric flow in cylindrical coordinates (r, θ, z) can be described as follows:

$$\vec{V}_c = V\,\mathbf{e_r} + U\,\mathbf{e_\theta} + W\,\mathbf{e_z} \tag{1}$$

Continuity:

$$\nabla \cdot \vec{V}_c = 0 \tag{2}$$

Momentum:

$$\rho_c \nabla \cdot \left(\vec{V}_c \vec{V}_c\right) = -\nabla p + \nabla \cdot \boldsymbol{\tau} \tag{3}$$

where $\vec{V}_c$ is the velocity field of the continuous phase, ρ_c its specific mass, p the pressure field and $\boldsymbol{\tau}$ the viscous stress tensor of a Newtonian fluid:

$$\boldsymbol{\tau} = \mu_c \left(\nabla \vec{V}_c + \nabla^T \vec{V}_c\right) - \frac{2}{3}\mu_c \mathbf{I} \nabla \cdot \vec{V}_c \tag{4}$$

where μ_c is the dynamic viscosity. The relative importance of viscosity can be described by the Reynolds number defined as $Re = \rho_c W_{avg} D / \mu_c$, where W_{avg} is the average axial velocity over the hydrocyclone cross section and D is the diameter (Fig. 1). The following dimensionless variables are also used: $p^* = p / \rho W_{avg}^2$, $U^* = U / W_{avg}$, $v^* = V / W_{avg}$, $W^* = W / W_{avg}$, $r^* = r / R$, $z^* = z / D$.

3. ANALYTICAL MODEL FOR THE DISPERSED PHASE

The dispersed phase (e.g. water) is assumed to consist of small particles spread out over the continuous phase. A simplified analytical model to predict the trajectory of a typical particle can be derived by assuming that the continuous phase is not influenced by the presence of small droplets. Besides, for sufficiently small drop sizes, the only difference between the velocity fields of the dispersed and continuous phases lies in the radial component. Assuming Stokes' law, the radial component of the particle velocity differs from the continuous phase by:

$$V_{r,d} = \frac{\rho_d - \rho_c}{18\mu_m} \frac{U^2 d_p^2}{r} \tag{5}$$

where the indexes d and c denotes dispersed and continuous phases, respectively, and d_p is the drop diameter. For fluid particles, the effective viscosity μ_m is given by Hadamard's expression

$$\mu_m = \mu_c \frac{\mu_d + \frac{2}{3}\mu_c}{\mu_d + \mu_c} \tag{6}$$

Assuming, for the sake of simplicity, that the velocity field of the continuous phase is of the form:

$$\vec{V}_c = U(z)\mathbf{e_\theta} + W\,\mathbf{e_z} \tag{7}$$

which, for $W = W_{avg} = const$ satisfies the continuity equation (2) immediately. Then, from the radial component of the momentum equation, the centrifugal force field capable of segregating the droplets is:

$$-\rho_c \frac{U^2}{r} = -\frac{\partial p}{\partial r} \tag{8}$$

The momentum equation in the tangential direction gives,

$$\rho_c W \frac{\partial U}{\partial z} = \frac{1}{r^2}\frac{\partial\left(r^2\tau_{r\theta}\right)}{\partial r} + \frac{\partial\tau_{z\theta}}{\partial z} \tag{9}$$

The last term of Eq. (9) can be neglected since, for sufficiently long hydrocyclones $\dfrac{\partial}{\partial z} << \dfrac{\partial}{\partial r}$. Taking the moment of Eq. (9) (i.e. multiplying by r) and integrating, the following result is reached:

$$\tau_{r\theta,wall}2\pi R^2 = \frac{d}{dz}\int_{r_i}^{R}(rU)\rho_c W 2\pi r dr \tag{10}$$

The integral appearing in Eq. (10) is directly related to the so-called Swirl number defined by (Gupta *et al.*,1984; Dirkzwager, 1996):

$$S = \frac{2\displaystyle\int_{r_i}^{r}(rU)\rho_c W \pi r dr}{\rho_c \pi R^3 W_{avg}^2} \tag{11}$$

where:

$$W_{avg} = \frac{1}{\pi R^2}\int_{ri}^{r}W 2\pi r dr \tag{12}$$

The swirl number is a dimensionless number that expresses the ratio of the axial flux of tangential momentum to the axial flux of axial momentum, thus it gives a measure of the strength of the swirling flow. As the flow develops downstream, wall friction reduces both the axial and tangential momentum fluxes in the near wall region (Baker and Sayre, 1971; Kitoh, 1991; Senoo and Nagata, 1972; Sheen *et al.*, 1996), thus causing swirl decay. From Eqs. (10-12), the rate of swirl decay becomes:

$$\frac{dS}{dz} = -\frac{2\tau_{r\theta,wall}}{\rho_c R W_{avg}^2} \tag{13}$$

where the shear forces and fanning friction factor can be introduced as:

$$\tau_{r\theta,wall} = \frac{1}{2}f_\theta\rho_c U^2(z) \tag{14}$$

$$f_\theta = K\left(\frac{\rho_c U_{avg}D}{\mu_c}\right)^{-n} \tag{15}$$

with K and n being dimensionless constants. For the continuous velocity field assumed in Eq. (7), the swirl number becomes:

$$S = \frac{2U}{3W_{avg}} = \frac{2U^*}{3} \tag{16}$$

and using Eqs. (14-16), Eq. (13) becomes:

$$\frac{dU^*}{dz^*} = -3K\,Re^{-n}\,U^{*(2-n)} \tag{17}$$

The $n = 1$ case corresponds presumably to laminar flow (linear effect of the viscosity). In this case, integration of Eq. (17) provides an exponential decay of the tangential velocity:

$$U^*(z^*) = U_i^* e^{-C_{decay}z^*} \tag{18}$$

where, $U_i^* = U^*(0)$ and $C_{decay} = -\dfrac{3K}{Re}$. Equation (18) is similar with the swirl decay obtained by Dirkzwager (1996). Nevertheless, it is questionable whether a dependency of the laminar type (n = 1) for the friction factor would be always appropriate, since the flow in a hydrocyclone is often turbulent. In steady state flow the trajectory of a single particle will be identical to a streamline passing by the same initial point. Thus, by integrating the condition $\dfrac{dr}{V_{r,d}} = \dfrac{dz}{W}$ with the help of Eqs. (5) and (18) leads to the following result:

$$r^*(z^*) = \sqrt{r_i^{*2} - \frac{4C_{drop}d_p^2 U_i^{*2}}{DC_{decay}W}\left(e^{-2C_{decay}z^*} - e^{-2C_{decay}z_i^*}\right)} \tag{19}$$

where r_i^* is the initial radial position of the drop at z_i^* and $C_{drop} = \dfrac{\rho_d - \rho_c}{18\mu_m}$.

4. NUMERICAL METHOD

The mass and momentum equations are solved using the finite volume technique (Patankar, 1980) embodied on the Phoenics® 2009 CFD code. The flow is considered to be steady, incompressible and axis-symmetric. A structured cylindrical polar grid properly describes the flow domain inside the settling zone. The orthogonal directions are X, Y and Z representing the tangential, radial and axial directions respectively, Fig. 1. The flow field has three velocity components: U, V and W, which correspond to the velocities along X, Y and Z.
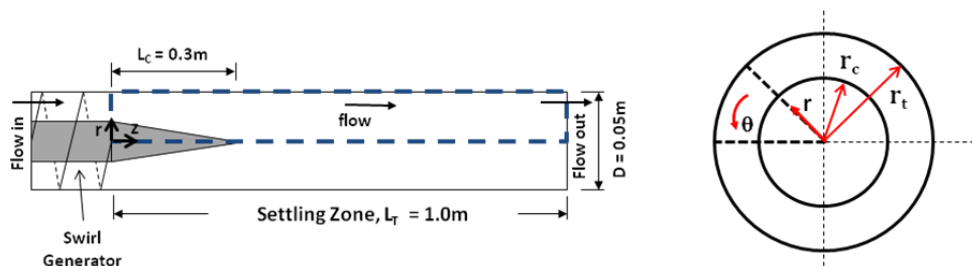

Figure 1. Swirling flow geometry

The domain size along X, Y and Z is, respectively, 1 rad, 0.025m and 1.0m. The structured orthogonal grid is non uniform along the Z direction. The influence of the grid size on the numerical results was assessed using three grid sizes, having 1587000, 2187000 and 2592000 control volumes. There are changes between the first and the second grid

but from the second to the third they are quite small indicating numerical convergence. The best result considering computational time was obtained for 2187000 control volumes. This set up is used in all simulations in this paper.

The boundary conditions used in this domain are: At r = R = D/2 the no-slip condition is used and at r = 0 the condition ∂/∂r = 0. The average axial component (W_{avg}) was transformed into a Reynolds number (*Re*) by rewriting the momentum equations in dimensionless form. Besides, every velocity component vanishes at the walls. Table 1 shows the boundary conditions adopted.

The annular thickness ratio, $\delta^* = (r_t - r_c)/r_t$, Fig. 1, was set to 0.2 and 0.4. At the inlet the axial and swirl inlet velocities are specified as W_{in} and U_{in}, which bear the relationship: $tg\,\alpha = W_{in}/U_{in}$, where α is the angle that the stationary blade makes with the axis line, α equals 63.43 and 72 degrees. For reference they are schematically represented in Fig. 2.

Viscosity and density of the continuous oil phase were set at 0.298 Pa.s and 937.8 kg/m^3 , respectively, and at 0.001 Pa.s and 998.2 kg/m^3 for the dispersed water phase, with droplet diameter of 1000µm. Simulations in this work were performed for *Re* = 500.

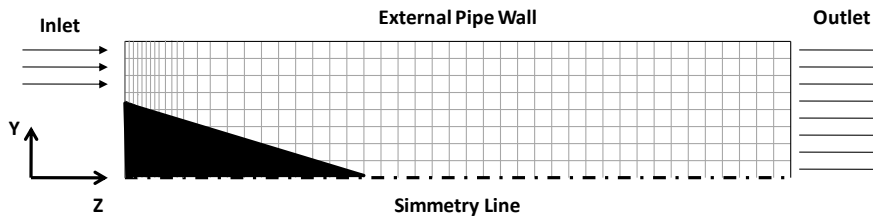**Figure 2.** Schematic of the grid

Table 1. Boundary Conditions

Inlet	Outlet	At r = 0	Wall (at r = R)
$U_{in} = W_{in}/tg(\alpha)$	$\dfrac{\partial u}{\partial z} = 0$	$\dfrac{\partial u}{\partial r} = 0$	$u = 0$
$V = 0$	$\dfrac{\partial v}{\partial z} = 0$	$\dfrac{\partial v}{\partial r} = 0$	$v = 0$
$W_{in} = \dfrac{Re\,\mu}{\rho D}\left[\dfrac{A}{A_{in}}\right]$	P_{rel}	$\dfrac{\partial w}{\partial r} = 0$	$w = 0$

The numerical solution stopped when the sum, over all control volumes, of the residuals of the mass and the momentum equations falls below 0.2% of the reference mass and momentum fluxes. For convenience, the reference momentum flux for the *X* and *Y* directions was also taken as equal to the reference momentum flux for the *Z* direction.

Numerical particle tracking

The trajectory of the particle is obtained through the solution of an Euler-Lagrangian system. The continuous phase is solved by the Eulerian frame and the trajectory is determined by Lagrangian frame of reference. The particle position is:

$$\vec{X} = \int_t^{t+\Delta t} \vec{V}_p\,dt \qquad (20)$$

where $\vec{X} = (X_p, Y_p, Z_p)$. In the present situation the forces acting on the particle are the force due to pressure gradient and the drag force. The forces due added mass and lift were neglected. The particle momentum equation is:

$$\rho_d \mathcal{V}_p \frac{d\vec{V}_d}{dt} = \rho_c \mathcal{V}_p \vec{g} + \frac{1}{2}\rho_c C_{drag}\left|(\vec{V}_c - \vec{V}_d)\right|(\vec{V}_c - \vec{V}_d\,)\mathcal{A}_p + \nabla\vec{p} \qquad (21)$$

where, to represent the centrifugal field, $\vec{g} = \dfrac{U^2}{r}\mathbf{e_r}$ and $\mathcal{V}_p, \mathcal{A}_p$ are the particle volume and cross area. The particle tracking is obtained by integrating Eqs. (20, 21) as functions of time, once the velocity field of the continuous phase is

solved. The algorithm used to obtain the trajectory of particles was the General Particle Tracking (Gentra) available in Phoenics®.

5. NUMERICAL RESULTS

Flow Field

Figure 3 illustrates the tangential velocities and axial velocities flow fields for Re = 500, annular thickness of 0.005m and $\alpha = 63.43^o$. The figure dimension is not in scale but magnified 2 times along tangential and radial directions, whereas the scale of axial direction was reduced by half.
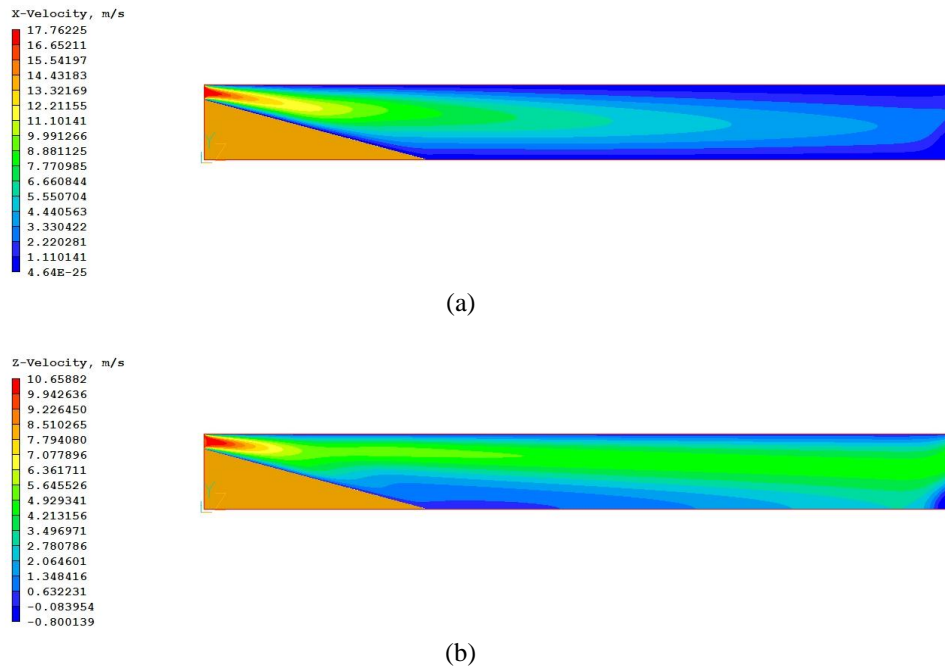
(a)

(b)

Figure 3. Velocity field: (a) Tangential Velocity ; (b) Axial Velocity

The tangential velocity in the inlet of the pipe is higher when the annular thickness is lower and its intensity decays with axial distance, as observed in Fig. 3a. Fig. 3b illustrates the axial velocities field. Negative values suggest an adverse pressure gradient in the region around Z = 6D.

The swirling flow field is governed by the behavior of the tangential component. The magnitude of the near-wall tangential velocity decreased with distance which can be explained by swirl decay and wall shear. Figure 3a illustrates the profile of the tangential velocity component at different axial positions. It can be observed that the swirl component increases with the radial position in the central region (as in a forced vortex), attains a maximum then decreases as the wall is approached. This behavior is not favorable for separating particles concentrated in the central region of the cyclone.

The development of the axial velocity downstream is shown in Fig. 4b for the same conditions of Fig. 3. At Z = 6D a central recirculation zone exists due to strong radial and axial pressure gradients caused by the expanding flow cross section area. Although the recirculation occurs, it is much smaller than that found in a previous work (Rocha, 2009). This should change the aspect ratio between the lengths of the cone and the tube. Murphy *et al*. (2007) has studied the turbulent swirling flow and also observed the formation of a central recirculation zone.
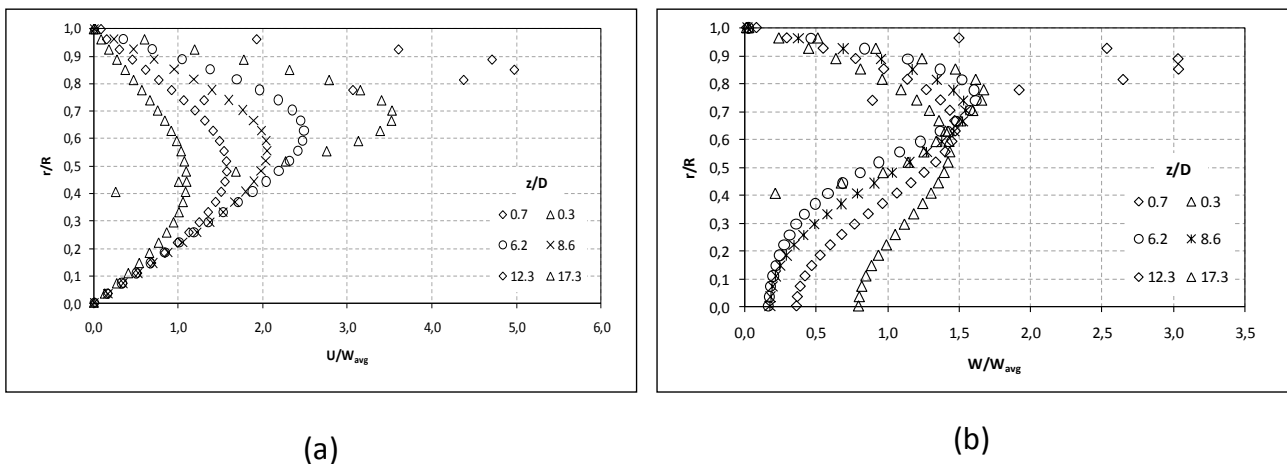
(a)

(b)

Figure 4. Tangential (a) and axial (b) velocity profiles at different axial positions for δ* = 0.2

Droplet Trajectory

The goal of the cyclone is the segregation of water droplets. Due to the assumption of a single phase flow field, the segregation calculations can be simplified by using the 'one-way coupling' approach. This means that the trajectories of the drops are influenced by the continuous phase flow field but the continuous phase is not influenced by the presence of the drops.

As an example, a series of tracks of d_p = 1000μm water droplets released at a range of radial locations is shown in Fig. 5. The droplets were released at coordinates (Y_i, Z_i) = (0.001m < y_i < 0.023m, 0.31m).

Droplets initially located at the center of the tube segregated at a radial position near 0.014 m. In a particular case, a droplet released at 0.001m from the symmetry line had 60% displacement in the radial direction.

Figure 6a illustrates the trajectory of a single water droplet of 1000μm size for Re = 500 and dimensionless annular thickness of 0.4 and 0.2. For smaller annular thickness, the particle migration is higher. This is because the tangential velocity component is greater when the annular thickness decreases, as observed previously (Rocha, 2009).
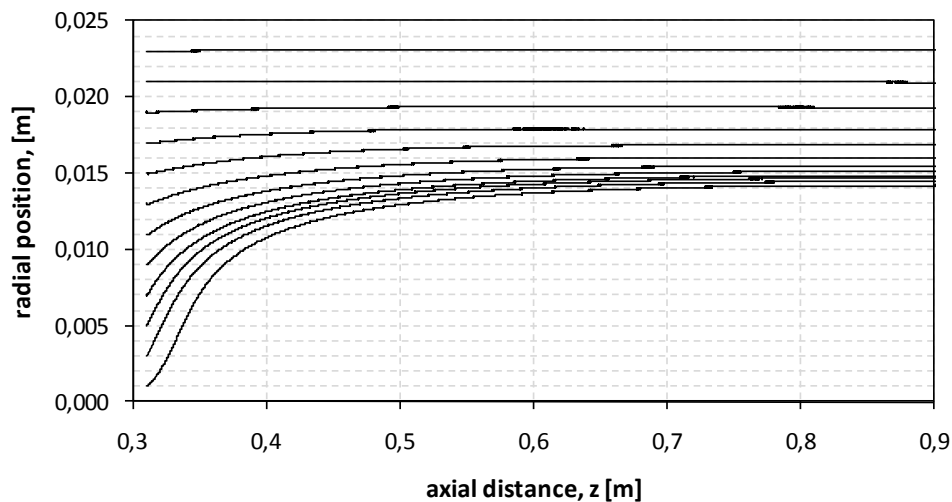

Figure 5. Trajectories of 12 1000μm size droplets for δ* = 0.2 and Re = 500.

Another parameter studied was the angle of the tangential velocity component at the pipe entrance. Two inlet angles were used two angles, 63.43 and 72 degrees. Figure 6b shows that using 63.43° the tangential velocity component is approximately two times greater than the axial velocity component. For an angle of 72°, the tangential velocity is approximately three times greater than the axial component of velocity. This result was expected since the larger the tangential velocity component, the higher the swirl number and, consequently, the greater the segregation. Despite this increase in segregation of the dispersed phase, one must beware that higher inlet angles also cause higher pressure drop through the inlet device.
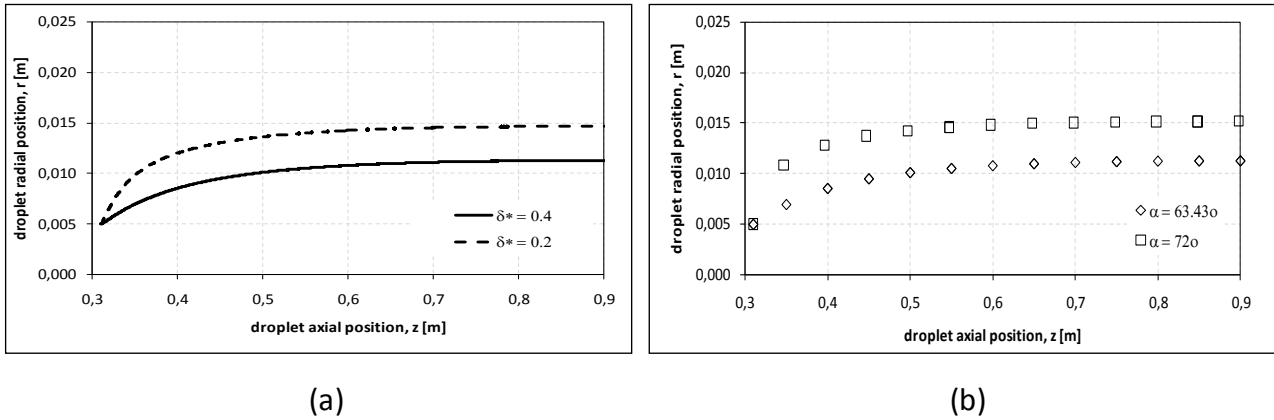
(a)

(b)

Figure 6. Effect of geometrical parameters on phase segregation: (a) annular thickness δ* and, (b) angle α.

Comparison between Numerical and Analytical Results

Figure 7a compares numerical tangential velocities with the model provided by Eq. (18) at different radial positions. The numerical results show that the tangential velocity is dependent of radial direction and agree with Eq. (18) only for a intermediate radial position r/R = 0.55. This could be expected because the assumption of uniform profile for the tangential velocity component is an over-simplification. Near the pipe center, r/R = 0.03, the tangential velocity decay is constant after z = 12D. Kitoh (1991), identified three regions in swirling flow: the wall region, dominated by sharps gradients, the annular region where the tangential velocity profile is dominated by a free vortex behavior and the core region where mean tangential velocity is maximum. The results of Fig. 7a seem to confirm this classification.

Figure 7b illustrates the swirl number decay along of length pipe. As the flow develops downstream, wall friction reduces both the axial and tangential momentum fluxes in the near wall region, thus causing swirl decay. In the present study, viscosity plays a prominent effect in swirl decay. The disagreement between numerical and analytical results is an indication that the effect of flow geometry on friction factor may be more complex than the proposed in Eq. (15).
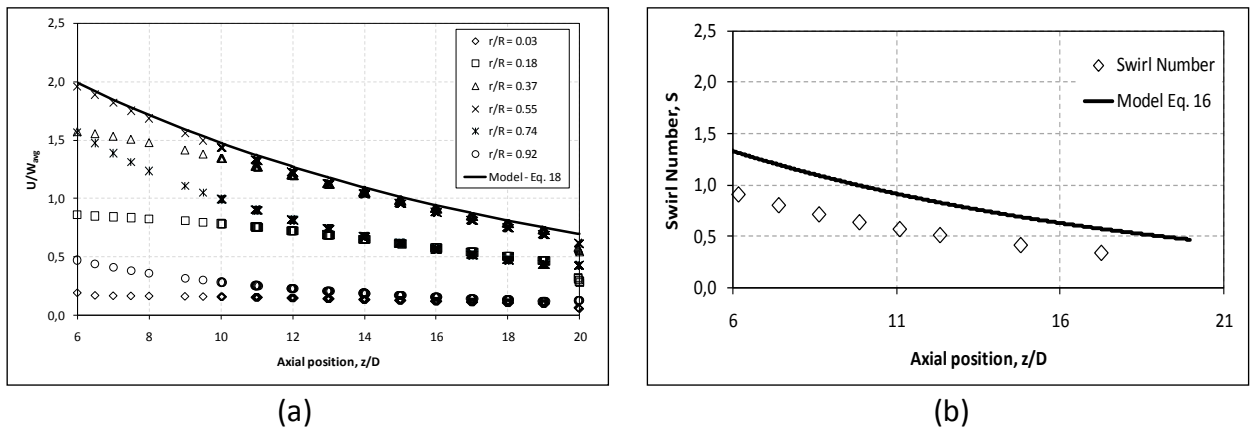

(a)

(b)

Figure 7. Analytical model *versus* numerical results: (a) Tangential velocity ; (b) Swirl number.

The numerical and analytical results for the droplet trajectories are compared in Fig. 10. There are good agreements between both solutions for $n = 1$ and $K = 12.5$. The analytical model and the numerical results are also compared with Dirkzwager (1996) results. Although the model uses a mean uniform tangential velocity profile in the cross section, still Eq. (19) predicts the water droplet trajectory very well. Selection of $n = 1$ in this case seems justified by the relatively low Reynolds number $Re = 500$, for which laminar flow can be presumed. The value of K was adjusted to 12.5, but it is not too far from the value 16 for fully developed pipe flow.
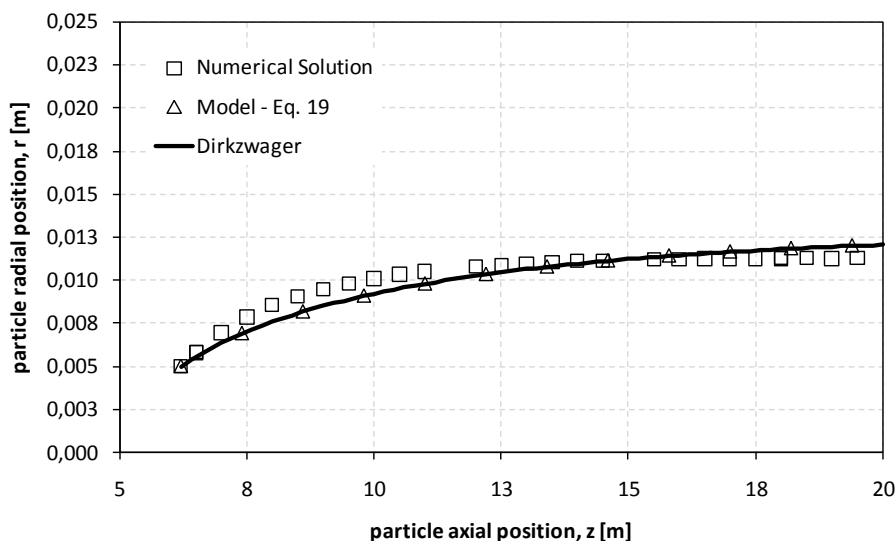
Figure 8. Trajectory of a 1000μm size droplet for $n = 1$ and $K = 12.5$

6. CONCLUSIONS

In the present work a numerical investigation of phase segregation in a liquid-liquid (oil-water) swirling flow axial hydrocyclone was performed by means of a CFD code. The effects of different geometrical parameters on phase segregation and droplet trajectories were investigated and the results were compared with the trajectories predicted by a rather simplified analytical. The flow was assumed to be laminar for applications in heavy oil-water separation. Numerical results indicate that, besides the inlet annular thickness, the inlet angle has a strong influence on the velocity profiles, pressure and swirl number evolutions along the hydrocyclone. The comparison suggested that higher angle presents advantage over smaller angles, although higher pressure drops in the inlet device can be expected.

Numerical and analytical model were compared for velocity profiles. The tangential velocity profile obtained numerically confirms the existence of regions found in the literature. For strongly swirling flow with initial swirl number greater than 1, the exponential decay predicted by the analytical model is only an approximation.

The water droplet trajectories in a continuous oil phase were very well predicted by the analytical model provided by Eq. (19). The next stages of the research will include simulations higher Reynolds numbers, typical of turbulent flow and the influence of wall friction law parameters.

7. ACKNOWLEDGEMENTS

8. REFERENCES

Baker,D. W., Sayre Jr., 1971, "Decay of swirling turbulent flow of incompressible fluids in long pipes", Flow its Measurement and Control in Science and Industry, Proceedings of the ASME Fluids Engineering Conference, v1, pp. 301-312.

Delfos, R., Dirkzwager, M., 1998, "Motion of oil droplets in strongly swirling pipe flow" Proceedings of 3rd International Conference on Multiphase Flow, Lyon, paper 445.

Delfos, R., Murphy, S., Stanbridge, D., Olujic, Z., Jansens, P. J., 2004, "A Design Tool for Optimising Axial Liquid-Liquid Hydrocyclones", Minerals Engineering, Vol. 17, pp. 721-731. Engineering Science, v62, pp. 1629-1635.

Dirkzwager, M., 1996, "A New axial cyclone design for liquid-liquid separation", Ph.D. Thesis, Delft University of Technology.

Gupta, A. K., Lilley, D. G., Syred, N., 1984, "Swirl Flows". Abacus Press, Turnbridge Wells.

Keege, S. J., 2000, "Numerical Simulation of an Axial Hydrocyclone", M.Sc. Thesis, Delft University of Technology.

Kitoh, O., 1991, "Experimental Study of Turbulent Swirling Flow in a Strainght Pipe", Jounal of Fluid Mechanics, v225, pp. 445-479.

Murphy, S., Delfos, R., Pourquié, M. J. B. M., Olujic, Z., Jansens, P. J., Nieuwstadt, F. T. M., 2007, "Prediction of Strongly Swirling Flow Within an Axial Hydrocyclones Using Two Commercial CFD Codes", Chemical Klujszo, L. A. C., Rafaelof, M., Rajamani, R. K., 1999, "Dust Collection Performance of a Swirl Air Cleaner", Powder Technology, Vol. 103(2), pp. 130-138.

Nieuwstadt, F. T. M, Dirkzwager, M., 1995, "A Fluid Mechanics Model for an Axial Cyclone Separator", Ind. Engineering Chemical Research, Vol.34, pp.3399-3404.

Patankar, S. V., 2009, "Numerical Heat Transfer and Fluid Flow", Hemisphere, Washington.

Rocha. A. D., "Numerical Study of Swirling Flow in a Liquid-Liquid axial Hydrocyclone Separator", 20th Int. Congress of Mechanical Engineering, Proceedings of Cobem, Gramado, Brazil.

Senoo, Y., Nagata, T., 1972, "Swirl Flow in Long Pipes with Different Roughness", Bulletin of the JSME, v15, pp.1514-1521.

Sheen, H. J., Chen, W. J., Jeng, S. Y., Huang, T.L., 1996, "Correlation of swirl number for a radial-type swirl generator". Experimental Thermal and Fluid Science, v12, pp.444-451.

Swanborn, R. A., 1998, "A New Approach to the Design of Gas-Liquid Separators for the Oil Industry", Ph.D. Thesis, Delft University of Technology.

Young, G. A. B., 1994, "Oil-Water Separation Using Hydrocyclone: An Experimental Search for Optimum Dimensions", Journal of Petroleum Science Engineering, Vol 11(1), pp 37-50.

8. RESPONSIBILITY NOTICE

The authors are the only responsible for the printed material included in this paper.